

Single proton particle stability with head-on beam-beam compensation in the RHIC

Y. Luo, W. Fischer and N. Abreu
Brookhaven National Laboratory, Upton, NY 11973, USA

To compensate the large tune shift and tune spread introduced by the head-on beam-beam interactions in the polarized proton (pp) run in the Relativistic Heavy Ion Collider (RHIC), we proposed a low energy electron beam with proper Gaussian transverse profiles to head-on collide the proton beam. In this article, with weak-strong beam-beam interaction model, we investigate the stability of single proton particle in the presence of head-on beam-beam compensation. Tune footprint, tune diffusion, Lyapunov exponent and 10^6 turn dynamic aperture are calculated and compared between the cases without and with beam-beam compensations. Tune scan and possibility of increasing bunch intensity are also studied.

1 Introduction

To maintain collisional beam lifetime and proton polarization in the polarized proton (pp) run in the Relativistic Heavy Ion Collider (RHIC), current working points for the proton beams are constrained between $2/3$ and $7/10$. It has been shown by both experiments and simulations that when the fractional betatron tune is close to $2/3$, the beam lifetime will be affected by the strong third order betatron resonances. And when the vertical tune is close to $7/10$, both the luminosity lifetime and proton polarization will be hurt. The nominal working points for the current pp runs are (28.685, 29.695) and (28.695, 29.685) for both RHIC rings. In the 2008 RHIC pp run, the bunch intensity had reached about 1.7×10^{11} . To further increase the bunch intensity to 2.0×10^{11} or even higher, there will be no enough tune space between $2/3$ and $7/10$ resonances to hold the large tune shift and tune spread generated by the proton-proton (p-p) head-on beam-beam interactions.

One solution is to adopt head-on beam-beam compensation. In the Tevatron at Fermi National Accelerator Laboratory, a low energy electron beam, usually called electron lens, or e-lens, has been introduced into the ring to compensate the long-range beam-beam interactions. Experimentally the long-range beam-beam compensation does increase the lifetime of PACMAN bunches in the bunch trains. In our study, we investigate if a device like the Tevatron e-lens can be used to mitigate the head-on beam-beam effects in the RHIC pp run.

To check the benefits and side effects from the head-on beam-beam compensation with e-lens in the RHIC, detailed simulation studies have to be done. In 2005, preliminary simulation study did show that e-lenses in the RHIC rings will greatly reduce the tune shift and tune spread generated by the p-head-on beam-beam interactions. However, more careful studies also have to be carried out to check its impacts on the collisional lifetime and emittance evolution of the proton beam.

In this article, we report the results from the study of stability of single proton particles in presence of head-on beam-beam compensation in the RHIC. We will first introduce the parameters of the proton and electron beams and the lattice for this study, followed by the beam-beam interaction model and tracking code we adopt. Then, we calculate and compare the tune footprint, tune diffusion and Lyapunov exponent from short term trackings and 10^6 turn dynamic apertures between the cases without and with head-on beam-beam compensations. In the end, we perform tune scan and check the possibility of increasing bunch intensity. The cause of the tune footprint foldings and comparison of two powerful tools, tune diffusion analysis and Lyapunov exponent analysis, are also shortly discussed.

2 Beam parameters and weak-strong beam-beam model

For the RHIC pp run, the two proton beams collide at IP6 and IP8. The proton beam in the Blue ring circulates clockwise, while the proton beam in the Yellow ring circulates anti-clockwise. In the current design

of RHIC head-on beam-beam compensation, e-lenses are put close to the crossing point IP10. Fig. 1 gives the layout the RHIC head-on beam-beam compensation.

Two e-lenses are needed for the RHIC head-on beam-beam compensation, one for the Blue ring and another one for the Yellow ring. The two proton beams are vertically separated in the interaction region (IR) of IP10. The e-lens for the Blue ring is named BEL, and the e-lens for the Yellow ring is named YEL. They are assumed 2 m long. They are symmetrically placed 1.5 meter away from IP10. However, in the following simulations, for simplicity, we assume the e-lenses are exactly located at IP10.

Tab. 1 lists the proton beam parameters in this study. The proton energy is 250 GeV, the relativistic factor is $\gamma = 266$. The beta functions at IP6 and IP10 are $\beta_{x,y}^* = 0.5$ m. The beta functions at IP10 where the e-lenses are are $\beta_{x,y}^e = 10$ m. The beta functions at other crossing points (IP2, IP4, IP10) are 10 m. In the simulation study, two uncollisonal working points, or nominal working points, (28.695, 29.685) and (28.685, 29.695), are used. The linear chromaticities are set to $Q'_{x,y} = +1$. The multipole magnetic field errors in the triplet quadrupoles and separation dipole magnets in the IRs are included in the lattice.

The bunch intensity is chosen as $N_p = 2.0 \times 10^{11}$. The proton beam rms transverse emittance is assumed to be 2.5 mm-mrad (15 mm-mrad for the 95% emittance). The normalized rms longitudinal bunch area of the proton beam is assumed to be 0.17 eV-s. The relative rms momentum spread of the proton beam is $\delta_{rms} = (\frac{\Delta p}{p_0})_{rms} = 0.14 \times 10^{-3}$, the rms bunch length of the proton beam is $\sigma_l = 0.44$ m.

For the best head-on beam-beam compensation, in this study we assume that the electron beam have same transverse Gaussian profiles as that of the proton beam at IP10. For the full head-on beam-beam compensation, the electron particle density is twice of that of proton bunch intensity, that is, $N_p = 4.0 \times 10^{11}$. For the half head-on beam-beam compensation, the electron particle intensity is $N_p = 2.0 \times 10^{11}$. Full and half head-on beam-beam compensations will compensate full and half linear beam-beam tune shifts, respectively.

In our following study, the 6-D symplectic tracking code SixTrack is used. In this code, the linear elements are treated as thick elements while the nonlinear elements are treated as thin-lenses. The beam-beam interaction calculation is based on weak-strong beam-beam interaction model. In our following study, for simplicity and calculation speed, 4-D beam-beam kick á la Basetti and Erskine is used. The beam-beam kicks from the electron beam on the proton particles are applied at IP10.

As a convention, we always launch initial particles for trackings in the first quadrant of $(x/\sigma_x, y/\sigma_y)$ plane. The initial conjugate momenta are set zero, $p_x = p_y = 0$. Initial coordinates of particles are sampled uniformly between 0° to 90° . In the calculations of tune footprints, tune diffusions and Lyapunov exponents, the initial coordinates of particles are sampled uniformly from zero to 6σ s. In dynamic aperture calculation fast binary searching is adopted.

In the following study, we calculate 4-D tune footprint, 4-D tune diffusion and 6-D Lyapunov exponent in 2048 turns to predicate the long-term stability of single proton particles. Limited by the computation capacity and computation round error, direct tracking to check single particle's long-term stability is carried out up to 10^6 turn. We assume that the regular particle motion is bounded for ever and the chaotic particle motion will diverge sooner or later. The long-term dynamic apertures will converge to the boundary between the regular and chaotic motions.

3 Tune footprint calculation in 4-D tracking

The initiate motivation of adopting e-lens for the RHIC pp run is to compensate the head-on beam-beam interaction generated tune shift and tune spread. The linear tune shift for the bunch core from p-p beam-beam interaction at one IP is given by

$$\xi = -\frac{N_p r_0}{4\pi\epsilon_n}. \quad (1)$$

Here N_p is the number of proton particles per bunch. r_0 is the classic radius of proton. ϵ_n is the normalized rms transverse emittance. ξ is also called beam-beam parameter.

The nominal tunes without collision are (28.685, 29.695) and (28.695, 29.685). Assuming the transverse normalized rms emittance $\epsilon_n = 2.5$ mm-mrad, the total beam-beam tune shift from two collisions at IP6 and IP8 with $N_p = 2.0 \times 10^{11}$ is about -0.02. Therefore, with $N_p = 2.0 \times 10^{11}$, the beam-beam tune shift will push the beam with uncollisonal working point (28.685, 29.695) to horizontal third order resonance line and push the beam with uncollisonal working point (28.695, 29.685) to vertical third order resonance line.

In this section, we calculate the tune footprints without and with beam-beam compensations. Initial particles are launched in the $(x/\sigma_x, y/\sigma_y)$ plane from $0\sigma_0$ to 6σ s with step 0.1σ and from 5° to 85° with step

Table 1: Parameters for the proton beams

quantity	unit	value
lattice		
ring circumference	m	3833.8451
energy	GeV	250
relativistic γ	-	266
beam-beam collision points	-	IP6, IP8
beam-beam compensation point	-	IP10
$\beta_{x,y}^*$ at IP6 and IP8	m	0.5
$\beta_{x,y}^e$ at IP10	m	10
$\beta_{x,y}^*$ at all other IPs	m	10
proton beam		
particles per bunch N_p	-	2×10^{11}
normalized transverse rms emittance $\epsilon_{x,y}$	mm·mrad	2.5
transverse rms beam size at collision points $\sigma_{x,y}^*$	mm	0.068
transverse rms beam size at e-lens $\sigma_{x,y}^e$	mm	0.31
transverse tunes (Q_x, Q_y)	-	(28.695, 29.685)
chromaticities (ξ_x, ξ_y)	-	(1, 1)
beam-beam parameter per IP $\xi_{p \rightarrow p}$	-	-0.01
longitudinal parameters		
harmonic number	-	360
rf cavity voltage	kV	300
rms longitudinal bunch area	eV·s	0.17
rms momentum spread	-	0.14×10^{-3}
rms bunch length	m	0.44

5°. The initial conjugate momenta are set to zero, $p_x = p_y = 0$. Each particle is tracked to 2048 turns. The betatron tunes are calculated with Sussix.

The top-left plot in Fig. 2 shows the footprints of on-momentum particles without and with head-on beam-beam interactions for both nominal working points. The footprints above the diagonal are for uncollisional working point (28.685, 29.695) and the footprints below diagonal is for uncollisional working point (28.695, 29.685). Different colors in Fig. 2 show the range of initial amplitudes. From the top-left plot of Fig. 2, with beam-beam interactions at IP6 and IP8, the beam with uncollisional working point (28.685, 29.695) is pushed onto horizontal third order resonances, while the beam with uncollisional working point (28.695, 29.685) is pushed onto vertical third order resonances. The beam-beam interactions also generate a much larger tune spread than the nonlinear magnetic fields.

The top-right plot in Fig. 2 shows the footprints of on-momentum particles with half and full head-on beam-beam compensations for both nominal working points. From the top-right plot in Fig. 2, the full and half head-on beam-beam compensation compensate full and half beam-beam tune shift. With head-on beam-beam compensation, the tune spreads generated by the proton-proton interactions are also greatly reduced. The particles in the bunch cores are pulled away from the third order betatron resonance lines. With full head-on beam-beam compensations, tune spreads are almost comparable to that without any beam-beam interaction.

In the top-right plot of Fig. 2, foldings in the tune footprints in radial and azimuthal directions are noticed, especially for the case with full beam-beam compensations. Without beam-beam interaction, there is no tune footprint folding up to 6σ . Only with p-p beam-beam interactions at IP6 and IP8, the tune footprint folding happens beyond 5σ . With half beam-beam compensation, it happens at 4σ . With full beam-beam compensation, the tune footprint foldings starts from a very small amplitude and the folding happens in both radial and azimuthal directions.

The two bottom plots in Fig. 2 show the tune footprints for the off-momentum particles. The relative momentum deviation is $\delta_p = \frac{\Delta p}{p_0} = 0.0005$ which is $3\sigma_p/p_0$. In our calculation, the first order chromaticities are set to $Q'_{x,y} = +1$. There is no significant difference in the shapes of tune footprints between on- and off-momentum particles.

In this section, we verified that head-on beam-beam compensations can greatly reduce the p-p beam-beam interactions generated large tune shift and tune spread. However, with head-on beam-beam compensations,

tune footprint foldings happen earlier at lower amplitudes, comparing to the case without beam-beam compensation. The cause and effect of beam-beam generated tune footprint foldings will be discussed later.

4 Tune diffusion calculation in 4-D tracking

In this section, we calculate and compare 4-D tune diffusion for on-momentum particles without and with beam-beam compensations. Tune diffusion analysis, or more generally called frequency map analysis, has been used for the study of single particle stability since J. Laskar introduced it from galaxy system into Accelerator Physics. Tune diffusion from short-term tracking is used as an indicator of long-term particle stability. If the particles motion is regular, its tune diffusion will be small. And if the particle motion is chaotic, its tune diffusion will be large. Normally tune diffusion is calculated in a 4-D tracking.

In our study, the initial particle coordinates are sampled uniformly from $0\sigma_0$ to 6σ s with 0.1σ and from 1° to 89° with step 1° in the $(x/\sigma_x, y/\sigma_y)$ plane. The initial conjugate momenta are set to zero, that is, $p_x = p_y = 0$. Each particle is tracked up to 2048 turns. The betatron tunes are calculated in the first and second 1024 turns. The tune diffusion in the 2048 turn is defined as

$$|\Delta Q| = \sqrt{|\Delta Q_x|^2 + |\Delta Q_y|^2}. \quad (2)$$

$|\Delta Q_x|$ and $|\Delta Q_y|$ are the horizontal and vertical betatron tune differences between the first and second 1024 turns. Again in our study, the tunes are accurately evaluated with Sussix.

The tune diffusion can be shown both in $(x/\sigma_x, y/\sigma_y)$ plane and $(Q_x - Q_y)$ tune plane. Different colors show the orders of tune diffusions. In our study, deep and light blue dots means that the particles they represent have tune diffusion below 10^{-5} and are considered very stable. The back dots mean the particles they represent have larger than 10^{-2} tune diffusions. These particles are subject to lose in a long-term tracking. The particles represented by the green and yellow dots are between the very stable and unstable cases.

Fig. 3 and Fig. 4 show the tune diffusions of on-momentum particles for working point (28.685, 29.695) and (28.695, 29.685) in the $(x/\sigma_x, y/\sigma_y)$ plane, respectively. In both figures, the top-left and top-right plots show the tune diffusions for the cases without and with p-p beam-beam interactions, respectively. The bottom-left and bottom-right plots show the tune diffusions for the cases with half and full head-on beam-beam compensations, respectively.

From Fig. 3 and Fig. 4, without beam-beam interactions, the tune diffusions for particles below 6σ s are below 10^{-4} . There is a large continuous deep and light blue area from zero to 4σ s. With p-p beam-beam interactions on, the large continuous blue area disappear. And several yellow curves with tune diffusion from 10^{-4} to 10^{-3} show up from zero up to $4-5\sigma$ s. Beyond $4-5\sigma$ s, there is a area scattered by some small yellow spots.

From Fig. 3 and Fig. 4, with head-on beam-beam compensations on, the tune diffusions for particles below 3σ s are reduced comparing to that without compensation. A small continuous blue area appears from zero up to $2-3\sigma$ s. With half beam-beam compensations, one or two green cures instead of yellow curves are visible below 3σ s. With full beam-beam compensation, the area above 4σ s with mixed colors (black, yellow and green colors) expands. More black dots are seen for the cases with beam-beam compensations.

The curves in yellow and green in Fig. 3 and Fig. 4 are actually linked to resonance structures. In Fig. 5, we plot the same tune diffusions in (Q_x, Q_y) tune space. Zooming into the tune footprints with half beam-beam compensation in Fig. 5, same resonances are visible before and after tune footprint foldings. Before foldings, the resonance line is colored in green with tune diffusion between 10^{-5} to 10^{-4} . After foldings, the same resonance line turns to back with tune diffusion above 10^{-2} . It is an evidence that foldings in the tune footprint should be avoided.

In Fig. 5, with p-p beam-beam interactions, the resonances are visible at low amplitudes. These yellow curves or resonances seem not to cause actual particle loss. With full beam-beam compensation, crossings of yellow curves are visible from very small amplitude. These resonance crossings produce the color-mixed area in Fig. 3 and Fig. 4. According to [], resonance crossing in the (Q_x, Q_y) plane, or resonance overlapping in $(x - px), (y - py)$ phase spaces indicate chaotic boundary. Below chaotic boundary is the so called dynamic aperture. Above the chaotic boundary, particles will lose sooner or later.

To conclude, from the tune diffusion analysis, head-on beam-beam compensations will help reduce the tune diffusions of particles below 3σ s. However, with beam-beam compensations, especially with full beam-beam compensation, resonance crossing or resonance overlapping happen earlier which reduces the boundary between the regular and chaotic motions and therefore the dynamic aperture.

5 Lyapunov exponent calculation in 6-D tracking

Lyapunov exponent is another indicator of single particle's long-term stability. By launching two adjacent particles with small enough distance in the phase space, the distance between these two particles will grow linearly or exponentially. The evolution pattern of the distance between these two particles in a short term tracking can be used to judge single particle's long-term stability.

According to Ref.[?], the maximal Lyapunov exponent in n th turn is defined as

$$\lambda(n) = \frac{1}{n} \ln \frac{|\mathbf{X}_2(n) - \mathbf{X}_1(0)|}{d_0}. \quad (3)$$

$\mathbf{X}_i(N)$, $i=1,2$, is the coordinate vectors of the two particles in the n th turn. The initial distance of these two particles in the phase space is $|\mathbf{X}_2(0) - \mathbf{X}_1(0)| = d_0$. d_0 should be originally very small to make the analysis meaningful. If the particle motion is regular or stable, the distance will grow linearly, and $\lambda(n)$ tends to zero. If the motion is chaotic or unstable, the distance of these two particles will grows exponentially and $\lambda(n)$ converges to a positive value.

In SixTrack, these two particles are called 'twin particles'. The difference in the twin particles' initial coordinates can happen in any directions of $(x, p_x, y, p_y, c\Delta t, \delta_p)$ phase space. In our study, the coordinate of first particle is uniformly sampled in the $(x/\sigma_x, y/\sigma_y)$ plane with zero conjugate momentum $p_x = p_y = 0$, from $0\sigma_0$ to 6σ with step 0.1σ and from 1° to 89° with step 1° . The second particle's coordinate differ from that of the first particle in x and y by $0.707e-06\text{mm}$. Then, the initial distance $d_0 = 10^{-6}\text{mm}$. Particles are tracked to 2048 turns. In our study, the longitudinal motion is turned on. However, for simplicity, we only calculate the maximal Lyapunov exponent in transverse planes.

As an example, Fig. 6 shows the distances and the maximal Lyapunov exponents for the regular and chaotic motions. The two top plots show the distances and the two bottom plots show the maximal Lyapunov exponents. The two left plots are for the regular motion. The two right plots are for the chaotic motion. From Fig. 6, the distance of the twin particles for the regular motion growth linearly and steadily. Its maximum Lyapunov exponent continues going down in 2048 turns. For the chaotic motion, the distance of the twin particles grows much faster and non-linearly. Two exponential growths are seen between 500-1200 turns and between 1600-2048 turns. As a result, its maximum Lyapunov exponent converge to a possible number in these parts. For simplicity, in the following, instead of showing $\lambda(n)$'s slope, we will plot $\lambda(2048)$ in the $(x/\sigma_x, y/\sigma_y)$ plane, which we call Lyapunov exponent map.

Fig. 7 and Fig. 8 show the maximum Lyapunov exponents in the $(x/\sigma_x, y/\sigma_y)$ plane for working points (28.685, 29.695) and (28.695, 29.685), respectively. In Fig. 7 and Fig. 8, the top-left and top-right plots show the maximum Lyapunov exponents without and with beam-beam interactions, respectively. The bottom-left and bottom-right plots show the maximum Lyapunov exponents with half and full beam-beam compensations, respectively. In each plot, dots with different colors show different ranges of $\lambda(2048)$. For example, the deep and light blue dots show the particles having $\lambda(2048)$ below 0.001. These particle motions are likely stable in long term tracking. The back dots show the particles with larger $\lambda(2048)$ than 0.003 and their motions are chaotic in a long-term tracking.

From top plots of Fig. 7 and Fig. 8, without beam-beam interactions, particles below 3σ are very stable. Pink dots are only seen beyond 5σ . There is no black dots up to 6σ . With p-p beam-beam interactions on, pink and red dots occupy the area from 1σ to 4.5σ . Below 1σ , some red dots are also visible there. Beyond 4.5σ , the area is filled with dots with different colors. Interestingly similar resonance curves from tune diffusion map are visible in the Lyapunov exponent map. Several black dots appear on the edges of these resonance strips.

From bottom plots of Fig. 7 and Fig. 8, with half head-on beam-beam compensations, the bunch core get more stable comparing to that without compensation. The pink dots dominate the area from 2σ to 3σ in the $(x/\sigma_x, y/\sigma_y)$ plane. With full beam-beam compensations, pink and read color dots are moved up from 3σ . Therefore, with half and full beam-beam compensation, the particles with small amplitudes get more stable than in the case of without compensation. However, it is noticed that with full beam-beam compensation, especially for working point (28.685, 29.695), there are more black dots appear above 4σ . These black dots gather on a wide resonance strip.

From the analysis of Lyapunov exponent maps, similar conclusion can be drawn as that from the above tune diffusion analysis. The head-on beam-beam compensation helps stabilize particles below 3σ but hurts particles beyond 4σ . With full beam-beam compensation, the boundary between the regular and chaotic motion is reduced to about 4σ .

6 Dynamic aperture calculation in 6-D tracking

In this section we calculate 6-D dynamic apertures without and with head-on beam-beam compensation. The dynamic aperture (DA) is defined as the maximum phase-space amplitude within which particles do not get lost in a certain tracking turn as a sequence of single-particle dynamic effects. The long-term dynamic aperture is supposed to converge to the boundary between the regular and chaotic motions. However, limited by computation capacity and computation wrong error, direct particle tracking beyond 10^7 seems difficult.

In the following, we search dynamic apertures in the $(x/\sigma_x, y/\sigma_y)$ plane in 10^6 turn trackings. The initial particles are sampled from 5° to 85° with step 5° , and from zero to 12σ with amplitude step 0.2σ . The particle's initial conjugate momenta are set to zero, $p_x = p_y = 0$. The longitudinal motion is on in this study.

There are some small difference in the dynamic apertures among the phase angles in the $(x/\sigma_x, y/\sigma_y)$ plane. To simplify comparison, we focus on the minimum dynamic aperture D_{min} and the phase averaged dynamic aperture D_{avg} among these phase angles. The phase averaged dynamic aperture is defined as

$$D_{avg} = \left(\sum_{i=1}^9 D(\alpha_i)^4 \sin(2\alpha_i) \Delta\alpha \right)^{\frac{1}{4}}. \quad (4)$$

$D(\alpha_i)$ is the dynamic aperture in phase space direction α_i , $\Delta\alpha$ is angle step among the phase angles.

Fig. 9 shows 10^6 turn dynamic apertures for both working points under different conditions. The top-left and top-right plots show the 10^6 turn dynamic apertures with the collisional working point (28.685, 29.695). The bottom-left and bottom-right plots show the 10^6 turn dynamic apertures with the uncollisional working point (28.695, 29.685). Alternatively, Fig. 10 shows dynamic apertures with same beam-beam conditions for different working points. The top-left and top-right plots show the dynamic apertures without and with beam-beam, respectively. The bottom-left and bottom-right plots show the dynamic apertures with half and full beam-beam compensations, respectively.

Table. 9 lists the 10^6 turn dynamic apertures found in each phase angle and the minimum and phase-averaged dynamic apertures among these 9 angles. According to Table. 9, for the same beam-beam conditions, the dynamic apertures for on- and off-momentum particles are slightly different. The differences normally are less 0.5σ . The relative momentum deviation for off-momentum particles is $\delta_p/p_0 = 0.0005$. In the following, we focus on the comparison of the dynamic apertures for off-momentum particles.

From Table. 9, for off-momentum particles, the minimum and angle averaged dynamic apertures without beam-beam interaction are about 7.6σ s and 8.5σ s for the working point (28.685, 29.695), and are about 8.0σ s and 8.8σ s for the working point (28.695, 29.685). With the beam-beam interactions at IP6 and IP8, the minimum and angle averaged dynamic apertures drop about 2σ s.

With head-on beam-beam compensations, for off-momentum particles, both minimum and angle averaged dynamic apertures are reduced, comparing to that without compensation. For working point (28.685, 29.695), the minimum and angle averaged dynamic apertures drop by 0.7σ and 0.3σ with half beam-beam compensation and drop by 1.1σ and 0.7σ with full beam-beam compensation, respectively. For working point (28.695, 29.685), the minimum and angle averaged dynamic apertures drop by 0.3σ and 0.1σ with half beam-beam compensation and by 0.3σ and 0.3σ with full beam-beam compensations. Therefore, with head-on beam-beam compensation, we see more dynamic aperture drops for working point (28.685, 29.695) than that for working point (28.695, 29.685).

To conclude, 10^6 turn dynamic aperture reduction is seen with head-on beam-beam compensations. This coincides with the above qualitative analysis with short-term tune diffusion and Lyapunov exponent. The dynamic apertures are linked to the boundary between the regular and chaotic particle motions in a long-term tracking. Dynamic aperture doesn't tell how stable the survived particles are. The drop in the dynamic aperture with head-on beam-beam compensation does hint the actual beam lifetime will be hurt.

7 Dynamic apertures in tune scan

In this section, we continue to calculate 10^6 dynamic apertures with beam-beam compensation in a tune scan. The tune scan is carried out along the diagonal in the tune space and the step of tune change is 0.005.

With half head-on beam-beam compensation, we calculate dynamic apertures for working points (28.685, 29.695) and (28.680, 29.690) above diagonal and for working points (28.695, 29.685) and (28.690, 29.680) below diagonal. With full head-on beam-beam compensation, we calculate dynamic apertures for working

Table 2: Dynamic apertures in 10^6 turn trackings

Case	D(5)	D(15)	D(25)	D(35)	D(45)	D(55)	D(65)	D(75)	D(85)	D_{min}	D_{avg}
WP685695-dp0:											
NoBB	9.3	9.3	8.0	8.2	7.9	7.3	8.4	9.0	9.2	7.3	8.3
BB	6.5	6.4	5.9	6.1	6.5	6.5	5.7	7.1	7.1	5.7	6.4
HBBC	6.3	7.9	6.0	5.6	6.2	6.0	5.8	6.0	6.8	5.6	6.2
FBBC	6.3	6.3	6.1	5.7	5.5	5.1	4.6	6.2	6.0	4.6	5.7
WP685695-dp5:											
NoBB	8.0	8.2	8.4	8.7	8.2	7.6	8.0	9.9	10.3	7.6	8.5
BB	6.6	6.4	6.5	6.8	6.9	6.4	6.5	8.0	7.7	6.4	6.8
HBBC	6.6	6.6	6.5	6.5	6.0	6.5	5.7	6.8	8.2	5.7	6.5
FBBC	6.4	6.6	6.4	6.1	5.3	5.7	5.8	6.8	6.7	5.3	6.1
WP695685-dp0:											
NoBB	10.1	8.8	8.0	7.3	8.0	8.4	8.2	7.8	9.0	7.3	8.2
BB	9.3	7.1	6.9	5.6	5.4	5.7	7.3	6.5	6.1	5.4	6.5
HBBC	9.2	7.2	6.5	5.6	5.7	5.7	7.1	6.5	6.1	5.6	6.5
FBBC	9.0	6.6	5.4	5.3	5.5	5.7	5.7	6.3	5.7	5.3	5.9
WP695685-dp5:											
NoBB	10.5	8.6	8.8	8.0	8.8	9.2	8.8	8.6	8.4	8.0	8.8
BB	9.8	7.7	6.9	6.1	6.1	6.2	7.2	7.2	6.8	6.1	6.9
HBBC	9.5	7.3	6.6	5.8	6.5	6.2	6.9	7.1	6.9	5.8	6.8
FBBC	10.1	7.1	6.0	6.0	6.1	5.8	7.1	6.7	6.9	5.8	6.6

points (28.685, 29.695), (28.680, 29.690) and (28.675, 29.685) above diagonal and for working points (28.695, 28.685), (28.690, 28.680) and (28.685, 28.675) below diagonal.

Fig. 11 and Fig. 12 show the dynamic apertures in the tune scan with half and full head-on beam-beam compensations, respectively. Table. 3 list all the calculated dynamic apertures in the tune scan. For each working point, dynamic apertures are calculated for on- and off-momentum particles. The relative momentum deviation for off-momentum particles is $\Delta p/p_0 = 0.0005$.

From Fig. 11 and Table. 3, with half head-on beam-beam compensation, there are very small changes in the phase averaged dynamic apertures in the tune scan. These changes are typically less than 0.2σ s, which is close to the resolution in our dynamic aperture searching. The difference in the minimum dynamic apertures are also small in the tune scan. In most cases, the minimum dynamic apertures differ by 0.1σ , except for the off-momentum particles in the above diagonal scan which gives 0.3σ change.

With full head-on beam-beam compensation, the changes in the tune scan in the phase averaged dynamic apertures are around 0.1σ in the tune scan. The only higher average dynamic aperture is for the on-momentum particle with working point (28.690, 29.680), which gives 6.3σ s. The minimum of the minimum dynamic apertures is given by the on-momentum particle with working point (28.685, 29.695). To conclude this section, there is no clear change in the 10^6 turn dynamic apertures in the above tune scans. In our tune scans, the lower tunes are all above 0.675.

8 Possibility of bunch intensity $N_p = 3.0 \times 10^{11}$

In the section we check the possibility of increasing bunch intensity. In the following, we assume the bunch intensity $N_p = 3.0 \times 10^{11}$ which gives about -0.03 beam-beam tune shift from p-p interactions at IP6 and IP8. We compensate two-third of the total p-p beam-beam tune shift with e-lens which gives the final beam-beam tune shift about -0.01 . For the 2/3 head-on beam-beam compensation for $N_p = 3.0 \times 10^{11}$, the required electron beam intensity from e-lens is 4.0×10^{11} , which is the same to that with full beam-beam compensation with $N_p = 2.0 \times 10^{11}$. If there is no significant proton beam lifetime drop with bunch intensity $N_p = 3.0 \times 10^{11}$ and 2/3 head-on beam-beam compensation, the luminosity will be doubled.

Fig. 13 and Fig. 14 shows the tune footprint, tune diffusion, Lyapunov exponent and dynamic aperture for working point (28.685, 29.695) and (28.695, 29.685) with bunch intensity $N_p = 3.0 \times 10^{11}$ and 2/3 head-on beam-beam compensation, respectively. Table. 4 lists the calculated 10^6 turn dynamic apertures.

From Fig. 13 and Fig. 14, with bunch intensity $N_p = 3.0 \times 10^{11}$ and 2/3 head-on beam-beam compensation,

Table 3: 10^6 turn dynamic apertures in the tune scan

Case	D(5)	D(15)	D(25)	D(35)	D(45)	D(55)	D(65)	D(75)	D(85)	D_{min}	D_{avg}
Half BBC, above diagonal:											
WP685695-dp0	6.3	7.9	6.0	5.6	6.2	6.0	5.8	6.0	6.8	5.6	6.2
WP680690-dp0	6.6	6.5	6.5	6.6	5.7	5.5	6.2	6.9	7.2	5.5	6.3
WP685695-dp5	6.6	6.6	6.5	6.5	6.0	6.5	5.7	6.8	8.2	5.7	6.5
WP680690-dp5	6.9	6.8	6.5	6.3	6.1	6.0	5.3	6.9	7.9	5.3	6.4
Half BBC, below diagonal:											
WP695685-dp0	9.2	7.2	6.5	5.6	5.7	5.7	7.1	6.5	6.1	5.6	6.5
WP690680-dp0	8.4	7.2	5.8	5.5	6.5	6.8	7.2	6.6	6.1	5.5	6.6
WP695685-dp5	9.5	7.3	6.6	5.8	6.5	6.2	6.9	7.1	6.9	5.8	6.8
WP685680-dp5	10.2	6.6	5.7	6.3	6.2	6.9	7.9	7.2	6.9	5.7	7.0
Full BBC, above diagonal:											
WP685695-dp0	6.3	6.3	6.1	5.7	5.5	5.1	4.6	6.2	6.0	4.6	5.7
WP680690-dp0	6.5	6.4	6.0	5.8	5.2	5.6	5.3	6.0	6.6	5.2	5.8
WP675685-dp0	6.5	6.4	6.3	5.8	5.2	5.5	5.2	5.9	6.2	5.2	5.8
WP685695-dp5	6.4	6.6	6.4	6.1	5.3	5.7	5.8	6.8	6.7	5.3	6.1
WP680690-dp5	6.9	6.8	6.2	5.9	5.7	6.1	6.0	5.7	7.4	5.7	6.1
WP675685-dp5	6.9	6.8	6.7	6.2	5.5	5.5	5.9	6.4	7.6	5.5	6.2
Full BBC, below diagonal:											
WP695685-dp0	9.0	6.6	5.4	5.3	5.5	5.7	5.7	6.3	5.7	5.3	5.9
WP690680-dp0	8.2	6.6	5.5	5.6	5.8	6.1	7.1	6.5	6.0	5.5	6.3
WP685675-dp0	8.0	6.3	4.9	5.3	5.4	6.3	6.5	6.2	5.8	4.9	6.0
WP695685-dp5	10.1	7.1	6.0	6.0	6.1	5.8	7.1	6.7	6.9	5.8	6.6
WP690680-dp5	7.6	6.2	6.4	5.2	5.7	6.2	7.8	7.2	6.9	5.2	6.5
WP685675-dp5	7.6	6.0	5.7	5.9	6.2	6.8	7.3	6.9	6.7	5.7	6.5

Table 4: 10^6 turn dynamic apertures with bunch intensity 3.0×10^{11}

Case	D(5)	D(15)	D(25)	D(35)	D(45)	D(55)	D(65)	D(75)	D(85)	D_{min}	D_{avg}
WP685695-dp0	6.1	6.1	5.6	5.4	5.4	5.4	5.7	5.7	5.6	5.4	5.6
WP685695-dp5	6.5	6.4	6.0	5.4	6.1	5.8	5.7	5.5	6.8	5.4	5.9
WP695685-dp0	9.3	6.3	5.7	5.1	5.5	5.4	6.1	6.2	5.8	5.1	6.0
WP695685-dp5	7.1	7.2	5.8	5.2	6.1	6.0	6.3	6.6	6.5	5.2	6.2

the beam-beam generated tune shifts are about 0.01. However, tune footprint foldings happen in both radial and azimuthal directions from very small particle amplitudes. From tune diffusion and Lyapunov exponent calculation, the black dots which represent irregular particle motions are seen starting from $2.5\sigma_s$.

From Table. 4, the 10^6 turn dynamic apertures for $N_p = 3.0 \times 10^{11}$ and 2/3 beam-beam compensation drop some, comparing to that for the nominal full beam-beam compensation shown in **Section 6**. For example,

To conclude this section, with increased bunch intensity $N_p = 3.0 \times 10^{11}$ and 2/3 head-on beam-beam compensation, the 10^6 turn dynamic aperture has a slight drop comparing to the nominal compensation scheme with bunch intensity $N_p = 2.0 \times 10^{11}$ and full beam-beam compensation. We expect more drop in the dynamic apertures in this case in extended tracking.

9 Cause for tune footprint folding

In this section we discuss the cause of tune footprint foldings. As an example, we calculate and show the horizontal tune shifts versus amplitude, or horizontal detunings, for on-momentum particles with working point (28.685, 29.695). All the detunings shown below are given with respect to the tunes for zero-amplitude particle.

The top-left plot in Fig. 15 shows the horizontal detuning only from the nonlinear magnetic fields. The top-right plot in Fig. 15 shows the detuning only from p-p beam-beam interactions at IP6 and IP8. The

proton bunch intensity is $N_p = 3.0 \times 10^{11}$. From them, there is no clear tune foldings in horizontal detuning in all phase angles. The detuning monopoly increase or decrease with the particle amplitude. This means that only nonlinear from the lattice or only p-p beam-beam interaction will not cause tune footprint foldings. We notice that the detuning from p-p beam-beam interactions increases much slowly and tend to get saturated after $5 - 6\sigma_s$ due to the fact that the particles beyond $5 - 6\sigma_s$ see less beam-beam force.

When the nonlinear magnetic fields from lattice and the beam-beam interaction are both turned on, if we simply add their detunings together, the total detunings are likely to fold sooner or later depending on how big the detuning from nonlinear magnetic fields is. If the detuning from nonlinear magnetic fields is big and the the beam-beam detuning is small (for example, with low bunch intensity), the tune footprint folding will come sooner. If the detuning from nonlinear magnetic fields is small and the beam-beam detuning is big, the tune footprint folding will happen later.

Another point is that the p-e head-on beam-beam compensation will complicate the situation. For example, with head-on beam-beam compensation in our case, the tune footprint foldings can happen only with p-p beam-beam interactions and p-e beam-beam compensation even without nonlinear in the lattice. With beam-beam compensation, together with nonlinear from lattice, tune footprint foldings are likely happen at a smaller particle amplitude.

Tune footprint foldings can happen in the azimuthal as well as in the radial directions in the $(x/\sigma_x, y/\sigma_y)$ plane. As an example, the bottom-left and bottom-right plots in Fig. 15 show the detunings with $N_p = 3.0 \times 10^{11}$ and 2/3 head-on beam-beam compensation in the radial and azimuthal directions, respectively. The foldings in the azimuthal direction is mainly caused by the different detunings from nonlinear magnetic fields in different phase angles. In our case, since the betas at IP10 and transverse emittances are very close, the detunings only from beam-beam interactions shouldn't give big difference in different phase angles.

To conclude, the tune footprint folding is caused by the beam-beam interactions together with the nonlinear magnetic fields. With head-on beam-beam compensation it will happen at smaller amplitude. It is not clear whether the tune footprint folding will happen only with nonlinear magnetic fields for the strong nonlinear lattice. It is also not clear to us how harmful the tune footprint folding will be. One evidence is that tune footprint foldings give opportunity to the resonance crossing and overlapping which should be avoided in the beam-beam study. Resonance crossing and overlapping normally hint the boundary between the regular and chaotic motions.

10 Tune diffusion map and Lyapunov exponent map

In the above studies, both tune diffusion and Lyapunov exponent in short term tracking are used as indicators of long-term stability of single proton particles. In this section, we will compare these two powerful tools.

Actually Lyapunov exponent has long been widely used to characterize the regular and chaotic motion. Lyapunov exponent analysis assumes that the distance between two particles originally very close in the phase space will increase linearly or exponentially depending on the motion is regular or chaotic. It can be used in 4-D or 6-D trackings. The resolution of this method is determined by the round-error in the tracking process. The tune diffusion analysis was introduced from galaxy system by Laskar in the late 1990's. This method depends on the accurate tune determination methods. It assumes that the more stable motion is, the less change in the betatron tunes. It is normally used in 4-d tracking since longitudinal motion will disturb the betatron tune evaluation.

From **Section 4** and **Section 5**, both tune diffusion map and Lyapunov exponent map reveal the resonance curves in the case of only with p-p beam-beam interactions at IP6 and IP8. The tune diffusion analysis is more powerful than the Lyapunov exponent to reveal resonance structures. Tune diffusion also discover resonance crossing or overlapping in the case of full beam-beam compensations.

Lyapunov exponent is sensitive to the diffusion in the spatial space. By tracking two particles originally very close in the space space, it directly tell the stability of particles in a long-term tracking. For example, in Lyapunov exponent map for the case of with full beam-beam compensation, the particles colored will back will lose sooner or later. Lyapunov exponent tell the result whether the particle will lose in a long-term tracking while the tune diffusion tells the reason why the particle motion is stable or chaotic.

However, at some time tune diffusion and Lyapunov exponent tell different story. For example, in the case of only with beam-beam compensation, below $4\sigma_s$, the particles in the center of resonance stripes have larger tune diffusions than particle on the edges of resonance strips. While from Lyapunov exponent component analysis, the particles in the center of resonance stripes have smaller Lyapunov exponents than that on the edge of the resonance strips. And in the Lyapunov exponent map, there is a larger red colored area around

coordinate $(2, 2)$ in the $(x/\sigma_x, y/\sigma_y)$ plane, while in the tune diffusion map these areas are colored with blue. This example shows that resonance sometime will not cause direct particle loss, especially for resonances at low amplitudes.

To conclude, tune diffusion is sensitive to the diffusion in the frequency domain while Lyapunov exponent is sensitive in the diffusion in the spatial domain. The tune diffusion analysis is more powerful than Lyapunov exponent to reveal resonance structures. However, Lyapunov exponent is the only one quantity to directly tell whether the particle will lose or not in a long-term tracking. And Lyapunov exponent can also be used in medium-term tracking while tune diffusion is mostly limited to short-term tracking. We suggest that both powerful methods should be used in the particle's long-term stability predication since Lyapunov exponent analysis tells the result while the tune diffusion analysis tells the reason.

11 Discussion

In the article, we calculated and compared the stabilities of single proton particles without and with head-on beam-beam compensation. From the calculated tune footprints, it is clear to show that head-on beam-beam compensation is very effective to reduce the p-p beam-beam generated large tune shift and tune spread.

Tune diffusion and Lyapunov exponent from 2048 turn tracking are used as indicators of long-term stability of single particle. Both studies show that head-on beam-beam compensation will stabilize the particles below $3\sigma_s$. This is understood since head-on beam-beam compensation reduces the tune shifts and pulls the particles in bunch core away from strong third order betatron resonances. And the particles in the bunch cores see less nonlinear effects introduced by the head-on beam-beam compensations.

Analysis of tune diffusion and Lyapunov exponent also show that head-on beam-beam compensation will hurt the stability of particles above $4\sigma_s$. Head-on beam-beam compensation cause the early happening of tune footprint foldings and earlier happening of resonance crossings or overlappings. Therefore, head-on beam-beam compensation reduces the boundary between regular and chaotic motions. This fact can be explained that head-on beam-beam compensation introduces more nonlinear forces into single particle dynamics in the range of 1σ to $5 - 6\sigma_s$. Below $6\sigma_s$, beam-beam effect gets weaker.

Limited by computation capacity and computation round error, 10^6 direct trackings are performed to search the so-called dynamic aperture. The dynamic aperture in a long-term tracking will eventually converge to the boundary between the regular and chaotic motions. Below that boundary, particle motion is bounded for ever. Above the boundary, particles are subject to lose sooner or later. In this study, we do see there are drops in the 10^6 turn dynamic apertures with head-on beam-beam compensation, comparing to that without beam-beam compensation.

In the article, we didn't check the stability of particles with small amplitudes through direct tracking. It is conjectured that the dynamic aperture is related to the real beam lifetime and the stability of the particles below $4\sigma_s$ will decide the real emittance growth rate. Beam lifetime and emittance growth are being studied with multi-particle tracking where about 10^4 macro-particle with 6-D Gaussian distributions are tracked up to 10^7 turns. Results will be reported in another article.

12 Conclusion

The stability of single proton particles in presence of head-on beam-beam compensation in the RHIC is studied carefully. Besides head-on beam-beam compensation can greatly reduce the p-p beam-beam interactions generated tune shift and tune spread, it also help stabilize the particles below $4\sigma_s$ since it pulls the particles in the bunch core away from strong third order resonances. However, we found that head-on beam-beam compensation will reduce the boundary between the regular and chaotic motions and therefore to reduce the overall beam lifetime. It is not clear at this moment how the head-on beam-beam compensation affect the bunch emittances, which is been studied with multi-particle trackings.

13 Acknowledgments

We are thankful for discussions with

This work is supported by the US DOE under contract No. DE-AC02-98CH10886.

References

- [1] V. Shiltsev and A. Zinchenko, “Electron beam distortions in beam-beam compensation setup”, Phys. Rev. ST Accel. Beams 1, 064001 (1998).

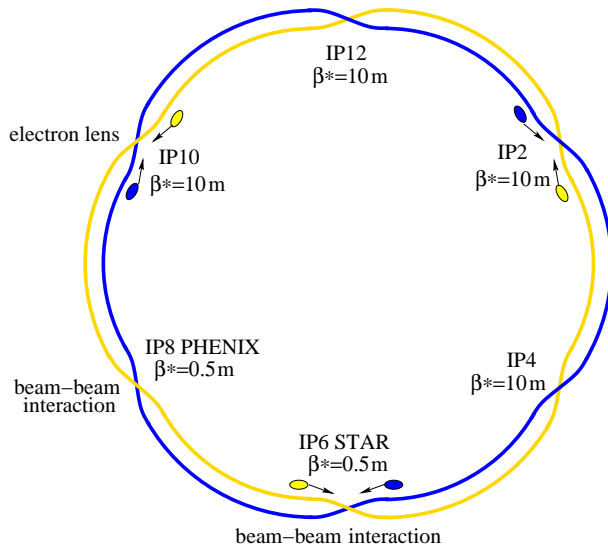


Figure 1: Layout for the simulation.

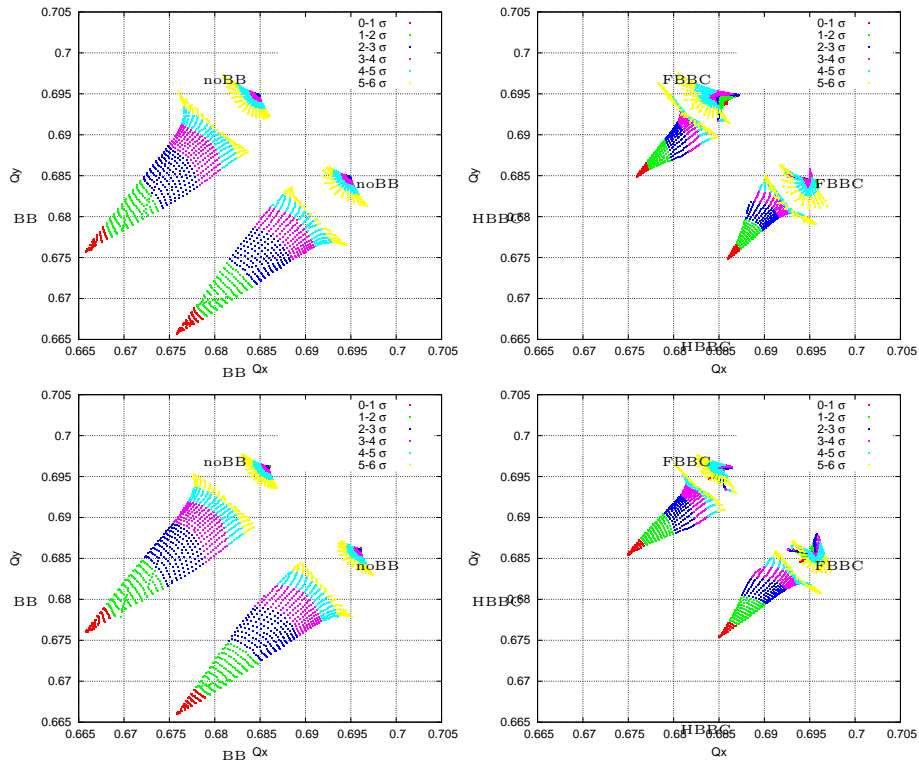


Figure 2: Tune footprints both working points. Top-Left: on-momentum particles without and with BB; Top-right: on-momentum particles with half and full BB compensations. Bottom-left: off-momentum particles without and with BB; Bottom-right: off-momentum particles with half and full BB compensations.

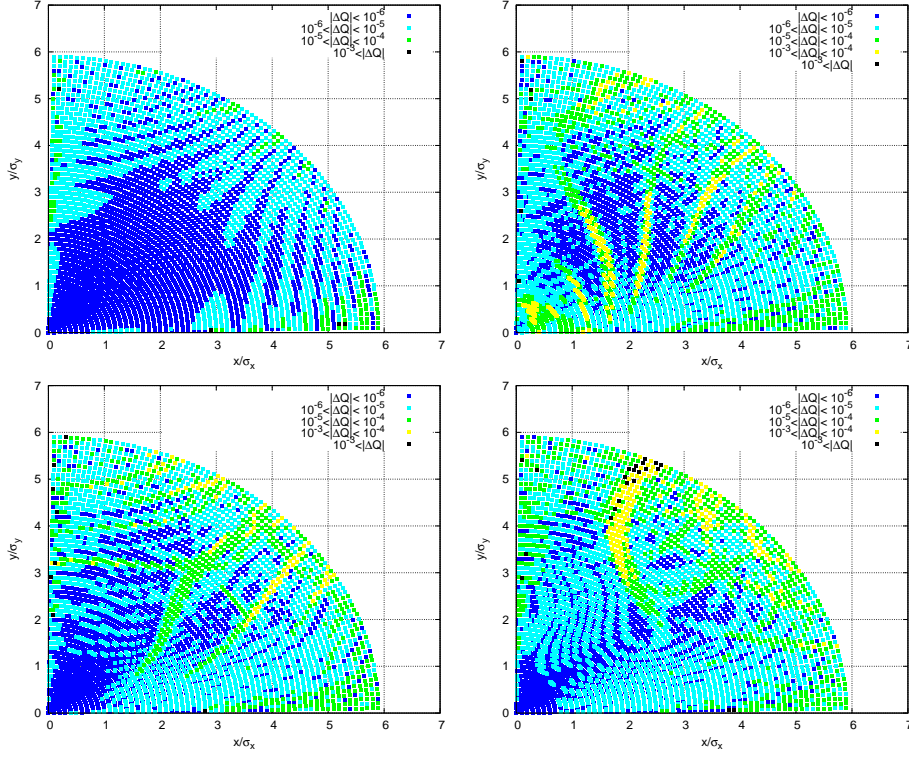


Figure 3: Tune diffusion maps of on-momentum particles for working point (28.685, 29.695): Top-left: without BB; Top-right: with BB; Bottom-left: with BB and half BB compensation; Bottom-right: with BB and full BB compensation.

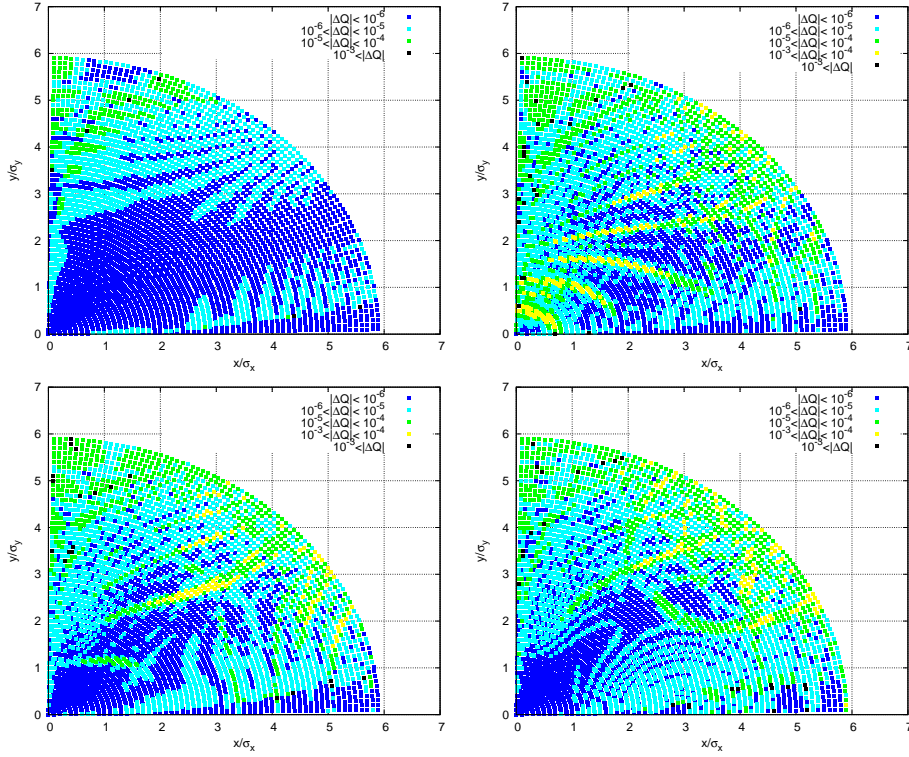


Figure 4: Tune diffusion maps of on-momentum particles for working point (28.695, 29.685): Top-left: without BB; Top-right: with BB; Bottom-left: with BB and half BB compensation; Bottom-right: with BB and full BB compensation.

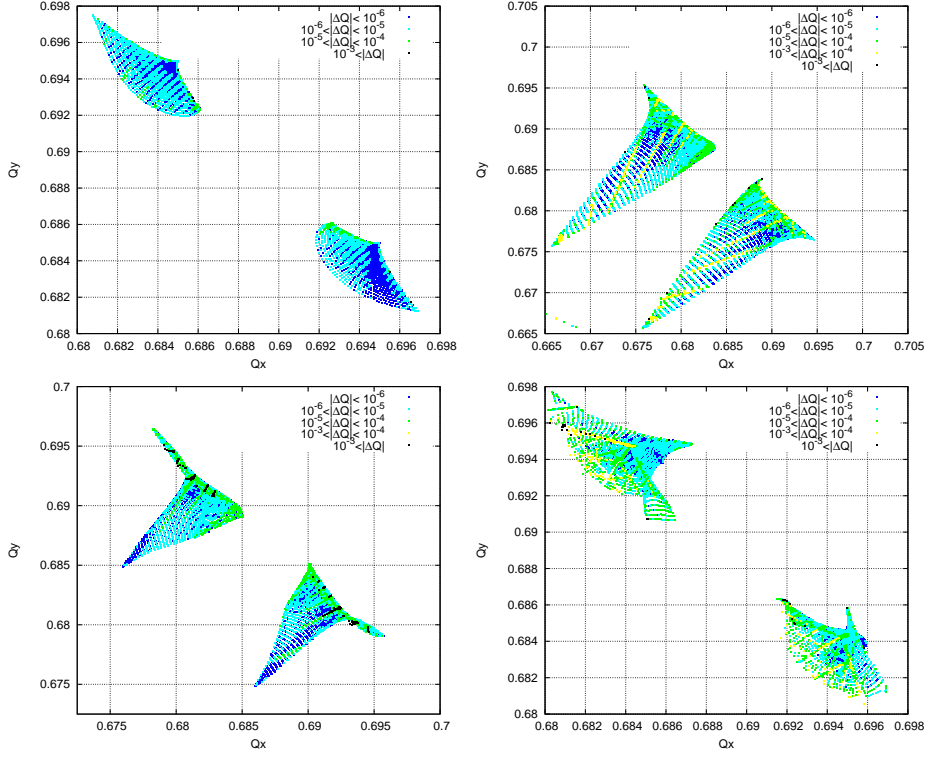


Figure 5: Tune diffusion maps of on-momentum particles in tune space for both working points: Top-left: without BB; Top-right: with BB; Bottom-left: with BB and half BB compensation; Bottom-right: with BB and full BB compensation.

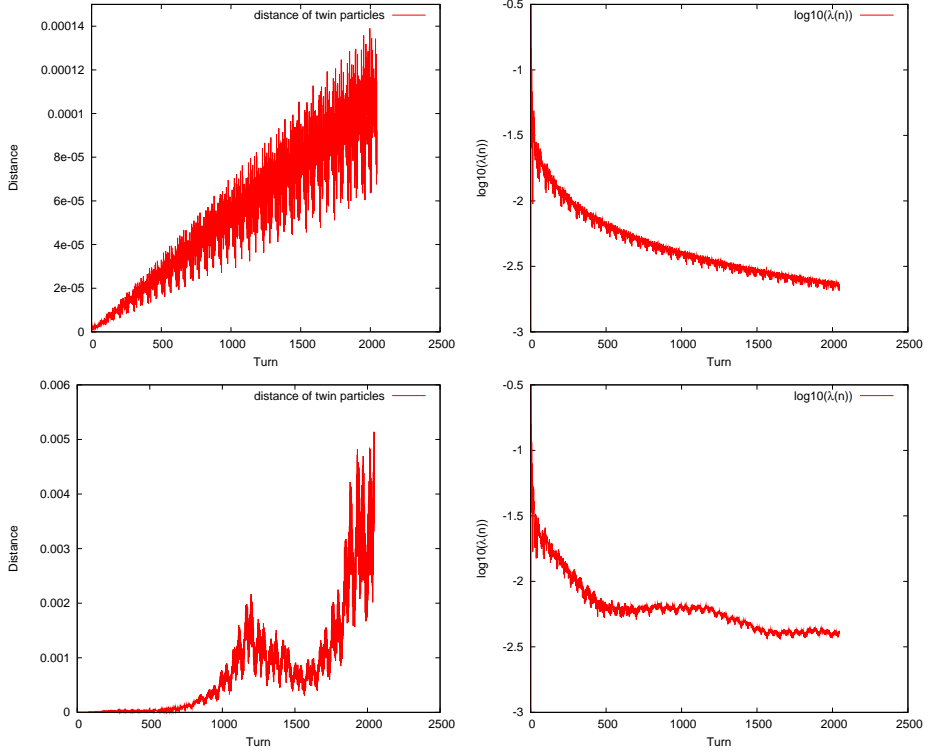


Figure 6: Example of Lyapunov exponents: Top-left and Top-right are the distance and $\lambda(n)$ of regular particle motion; Bottom-left and Bottom-right are the distance and $\lambda(n)$ of unregular particle motion. Tracking condition for the regular particle motion: WP685695-noBB, $6\sigma_s/45^\circ$; Tracking condition for the unregular particle motion: WP685695-BB-FBBC, $6\sigma_s/45^\circ$.

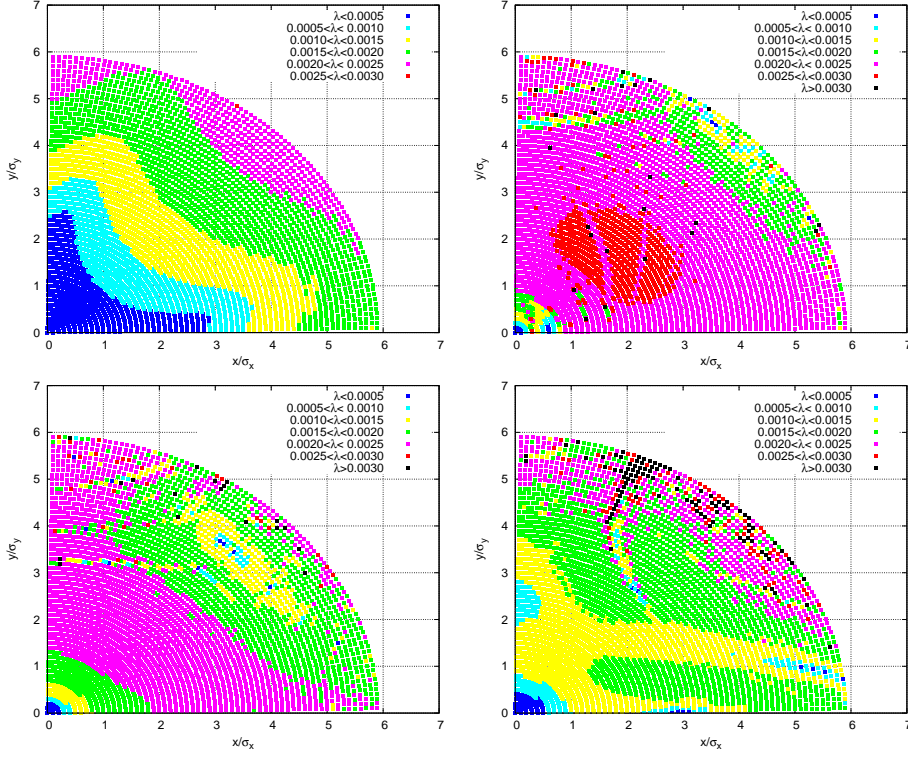


Figure 7: Lyapunov component maps of on-momentum particles for working point (28.685, 29.695): Top-left: without BB; Top-right: with BB; Bottom-left: with BB and full BB compensation; Top-right: with BB and half BB compensation.

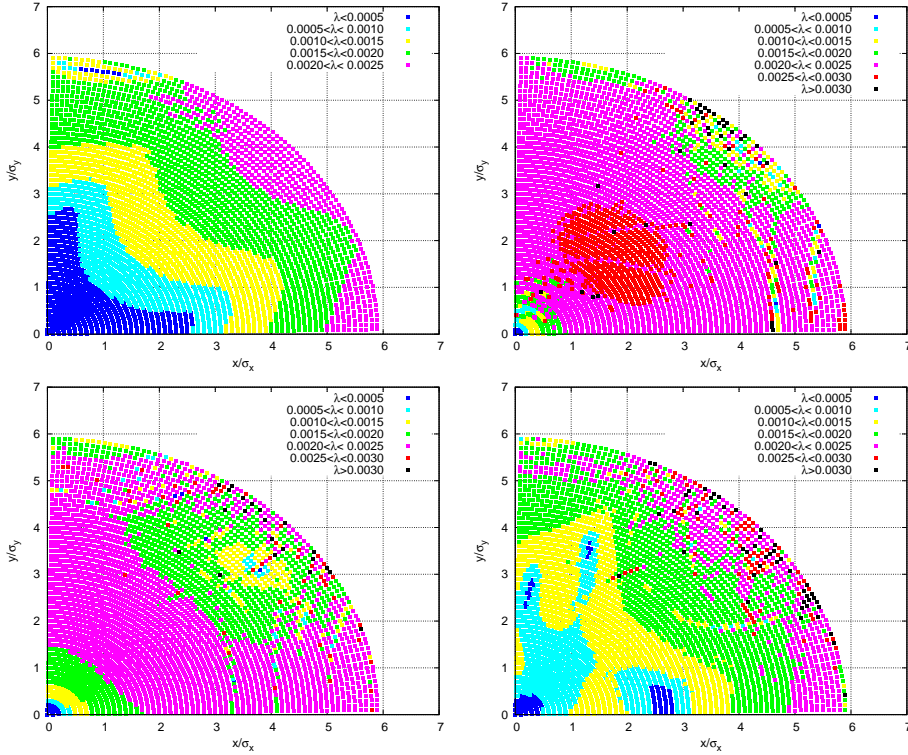


Figure 8: Lyapunov component maps of on-momentum particles for working point (28.695, 29.685): Top-left: without BB; Top-right: with BB; Bottom-left: with BB and full BB compensation; Top-right: with BB and half BB compensation.

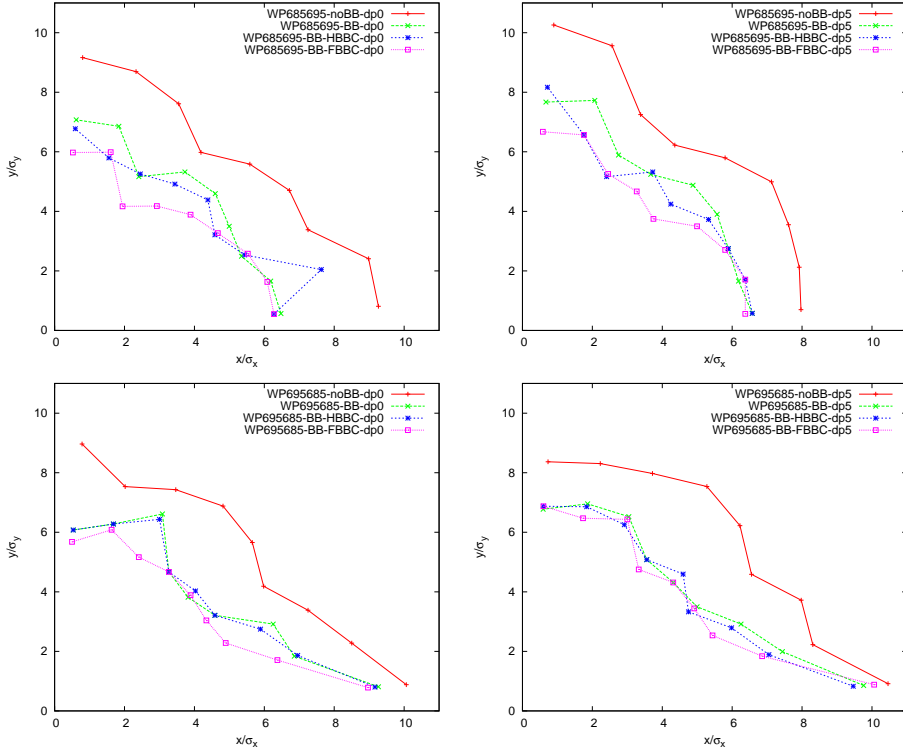


Figure 9: 10^6 turn dynamic apertures for both working points. Top-left: on-momentum particle with working point (28.685, 29.695); Top-right: off-momentum particle with working point (28.685, 29.695); bottom-left: on-momentum particle with working point (28.695, 29.685); bottom-right: off-momentum particle with working point (28.695, 29.685).

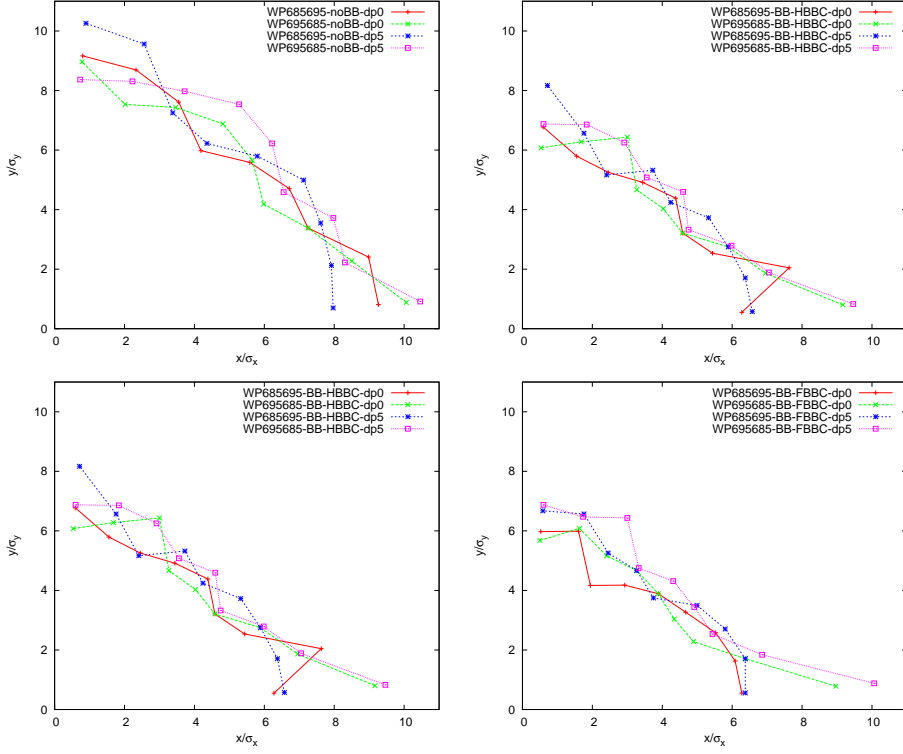


Figure 10: Comparing 10^6 turn dynamic apertures. Top-left: without beam-beam; Top-right: with beam-beam interactions at IP6 and IP8; bottom-left: with beam-beam interactions at IP6 and IP8 plus half beam-beam compensation at IP10 ; bottom-right: with beam-beam interactions at IP6 and IP8 plus full beam-beam compensation at IP10 .

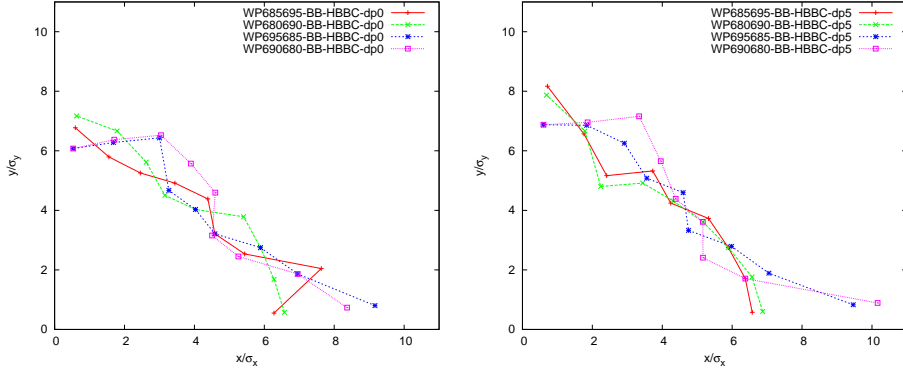


Figure 11: Tune scan with BB-HBBC.

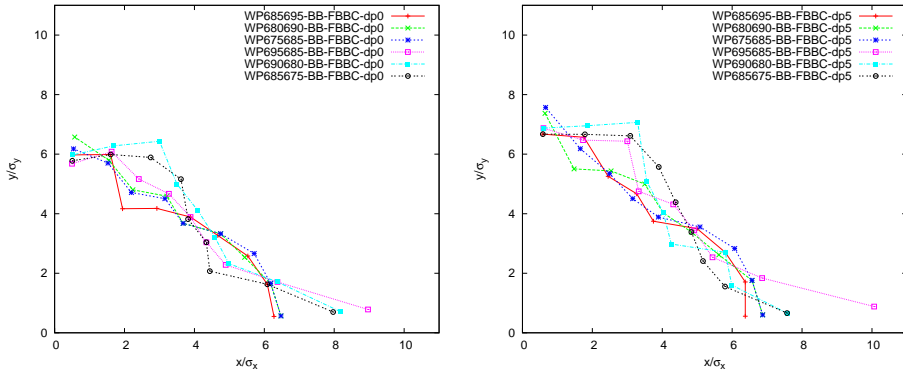


Figure 12: Tune scan with BB-HBBC.

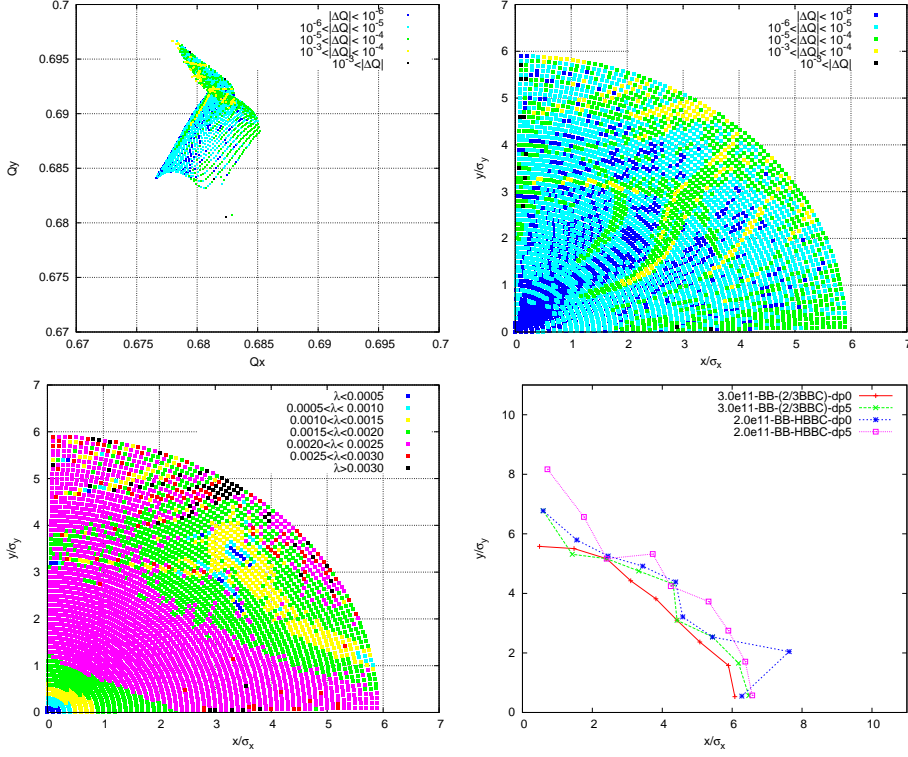


Figure 13: Tune footprint, Tune diffusion, Lyapunov exponent, and dynamic apertures with $N_p = 3.0 \times 10^{11}$ and 2/3 BBC for working point (28.685, 29.695).

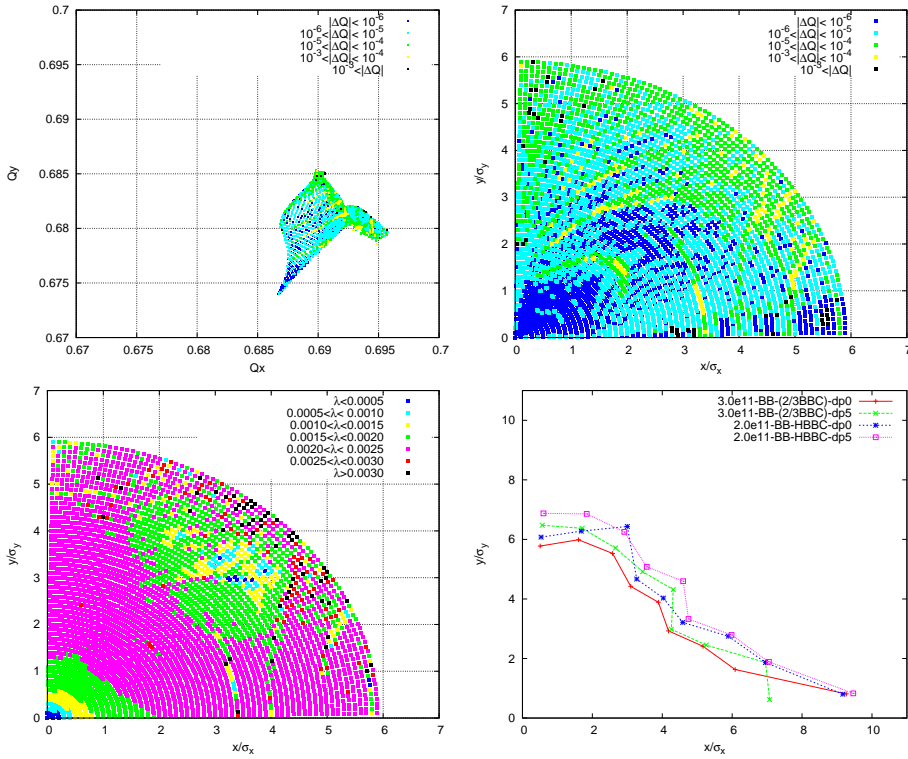


Figure 14: Tune footprint, Tune diffusion, Lyapunov exponent, and dynamic apertures with $N_p = 3.0 \times 10^{11}$ and 2/3 BBC for working point (28.695, 29.685).

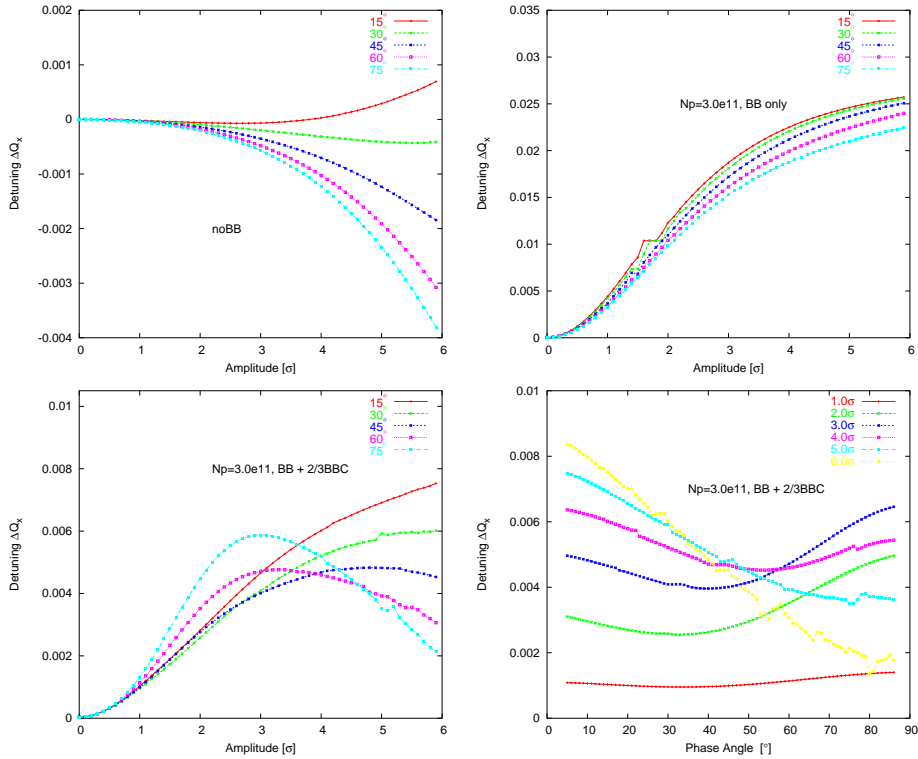


Figure 15: Examples of tune footprint foldings, working point is $(28.685, 29.695)$. Top-left: detuning ΔQ_x only from magnetic nonlinearities; Top-right: detuning ΔQ_x only from beam-beam interaction; Bottom-left: radial detuning ΔQ_x with $N_p = 3.0 \times 10^{11}$ and 2/3 head-on beam-beam compensation ; Bottom-right: azimuthal detuning ΔQ_x with $N_p = 3.0 \times 10^{11}$ and 2/3 head-on beam-beam compensation.